Eur. Phys. J. C (2017) 77:145
DOI 10.1140/epjc/s10052-017-4715-y

THE EUROPEAN PHYSICAL JOURNAL C

Letter

Next-to-leading order QCD predictions for top-quark pair production with up to three jets

S. Höche[1,a], **P. Maierhöfer**[2,b], **N. Moretti**[3,c], **S. Pozzorini**[3,d], **F. Siegert**[4,e]

[1] SLAC National Accelerator Laboratory, Menlo Park, CA 94025, USA
[2] Physikalisches Institut, Albert-Ludwigs-Universität Freiburg, 79104 Freiburg, Germany
[3] Physik-Institut, Universität Zürich, 8057 Zurich, Switzerland
[4] Institut für Kern- und Teilchenphysik, TU Dresden, 01062 Dresden, Germany

Received: 9 August 2016 / Accepted: 21 February 2017 / Published online: 7 March 2017
© The Author(s) 2017. This article is published with open access at Springerlink.com

Abstract We present theoretical predictions for the production of top-quark pairs with up to three jets at the next-to leading order in perturbative QCD. The relevant calculations are performed with SHERPA and OPENLOOPS. To address the issue of scale choices and related uncertainties in the presence of multiple scales, we compare results obtained with the standard scale $H_T/2$ at fixed order and the MINLO procedure. Analyzing various cross sections and distributions for $t\bar{t}+0,1,2,3$ jets at the 13 TeV LHC we find a remarkable overall agreement between fixed-order and MINLO results. The differences are typically below the respective factor-two scale variations, suggesting that for all considered jet multiplicities missing higher-order effects should not exceed the ten percent level.

1 Introduction

The top quark as the heaviest known elementary particle plays a fundamental role, both in the Standard Model and in new physics scenarios. Experimental analyses of Large Hadron Collider (LHC) data collected during run II will provide an unprecedented reach at high energy and in exclusive phase-space regions with associated production of jets and vector bosons or Higgs bosons. The production of a $t\bar{t}$ system in association with multiple jets plays an especially important role as a background to new physics searches and to various Higgs and Standard Model analyses. In particular, the precise theoretical control of $t\bar{t}$+multijet backgrounds is one of the most important prerequisites for the observation of top-quark production in association with a Higgs boson, which would give direct access to the top-quark Yukawa coupling. In addition, $t\bar{t}$+multijet production allows for powerful test of perturbative QCD and is also routinely exploited for the validation of Monte Carlo tools that are used in a multitude of LHC studies. All these analyses require theoretical predictions at the highest possible accuracy.

Inclusive top-quark pair production at hadron colliders has been computed fully differentially to next-to-next-to-leading order (NNLO) in the strong coupling expansion [1,2]. Predictions for top-quark pair production in association with up to two jets are available at the next-to-leading order (NLO) [3–8], and NLO calculations for inclusive top-quark pair production and in association with up to one or two jets were matched to parton showers in order to provide predictions at the particle level [9–18].

In this letter we report on the first computation of top-quark pair production with up to three jets at NLO QCD. At present only few scattering processes with more than six external legs are known at NLO [19–26], and the calculation at hand is the first one that deals with a $2 \to 5$ process with seven colored external particles including also heavy quarks. Detailed predictions are presented for $pp \to t\bar{t} + 0,1,2,3$ jets with stable top quarks at 13 TeV, both at the level of cross sections and differential distributions. We also investigate the scaling behavior of $t\bar{t}$+multijet cross sections with varying jet multiplicity.

The characteristic scales of $t\bar{t}$+multijet production, i.e. the invariant mass of the $t\bar{t}$ system and the transverse momentum threshold for jet production, are typically separated by more than one order of magnitude, while differential observables involve multiple scales, which can be distributed over

[a] e-mail: shoeche@slac.stanford.edu
[b] e-mail: philipp.maierhoefer@physik.uni-freiburg.de
[c] e-mail: moretti@physik.uzh.ch
[d] e-mail: pozzorin@physik.uzh.ch
[e] e-mail: frank.siegert@cern.ch

more than two orders of magnitude. In this situation, finding renormalization and factorization scales that ensure a decent convergence of perturbative QCD for the widest possible range of observables is not trivial. Moreover, in the presence of a wide spectrum of scales, the usage of standard factor-two variations for the estimation of theoretical uncertainties due to missing higher-order effects becomes questionable. Motivated by these observations, to gain more insights into the scale dependence of $t\bar{t}$+multijet production and related uncertainties we compare a fixed-order calculation, with the standard scale choice $H_T/2$, against results based on the MINLO method [27]. The scale $H_T/2$ was found to yield stable and reliable NLO predictions for V+multijet production [28], while the MINLO method is especially well suited for multi-scale QCD processes, as it controls, through next-to-leading logarithmic[1] (NLL) resummation, the various higher-order logarithms that emerge from soft and collinear effects in the presence of widely separated scales. The present study provides a first systematic comparison of the two approaches.

2 Details of the calculation

Our calculations are performed using the event generator SHERPA [29,30] in combination with OPENLOOPS [31,32], a fully automated one-loop generator based on a numerical recursion that allows the fast evaluation of scattering amplitudes with many external particles. For the reduction to scalar integrals and for the numerical evaluation of the latter we used CUTTOOLS [33] in combination with ONELOOP [34] and, alternatively, the COLLIER library [35], which implements the methods of [36–38]. Tree amplitudes are computed using COMIX [39], a matrix-element generator based on the color-dressed Berends–Giele recursive relations [40]. Infrared singularities are canceled using the dipole subtraction method [41,42], as automated in COMIX, with the exception of K- and P-operators that are taken from the implementation described in [43]. COMIX is also used for the evaluation of all phase-space integrals. Analyses are performed with the help of RIVET [44].

We carry out a series of $pp \to t\bar{t} + N$ jet NLO calculations with $N = 0, 1, 2, 3$, taking into account the exact dependence on the number of colors, $N_c = 3$. As an illustration of the rapid growth of complexity at high jet multiplicity, in Table 1 we list the number of one-loop Feynman diagrams that contribute to a few representative partonic channels. In addition to the presence of more than 10^5 loop diagrams in the $gg \to t\bar{t} + 3g$ channel, we note that also the very large number of channels not listed in Table 1 as well as the computation of real contributions pose very serious challenges in the $t\bar{t} + 3$ jet calculation.

Table 1 Number of one-loop Feynman diagrams in representative partonic channels in $pp \to t\bar{t} + N$ jets for $N = 0, 1, 2, 3$

Partonic channel\N	0	1	2	3
$gg \to t\bar{t} + N\,g$	47	630	9438	152,070
$u\bar{u} \to t\bar{t} + N\,g$	12	122	1608	23,835
$u\bar{u} \to t\bar{t}u\bar{u} + (N-2)\,g$	–	–	506	6642
$u\bar{u} \to t\bar{t}d\bar{d} + (N-2)\,g$	–	–	252	3321

Proton–proton cross sections are obtained by using, both at LO and NLO, the CT14 NLO PDF set [45] with five active flavors, and the corresponding strong coupling. Matrix elements are computed with massless b-quarks, and top quarks are kept stable. Hence, our results can be compared to data only upon reconstruction of the $t\bar{t}$ system and extrapolation of fiducial measurements to the full phase space. However, we expect the main features shown in our analysis to be present also in computations including top-quark decays and acceptance cuts. The latter will undoubtedly play a role, but the reduction of scale uncertainties is generic as long as the radiative phase space is not heavily restricted by experimental cuts. Apart from performing a direct analysis, we also provide Root NTuples [46] that can be used in the future for more detailed studies including top-quark decays and matching to parton showers.

In our standard perturbative calculations we employ renormalization and factorization scales defined as $\mu_R = \mu_F = H_T/2$, where $H_T = \sum_i \sqrt{p_{T,i}^2 + m_i^2}$, with the sum running over all (anti)top quarks and light partons, including also real radiation at NLO. Results generated in this manner are compared to alternative computations based on the MINLO procedure [27]. To this end, we have realized a fully automated implementation of the MINLO method in SHERPA.

3 MINLO method and implementation

The MINLO method can be regarded as a generalized scale setting approach that guarantees a decent perturbative convergence for differential multijet cross sections. This is achieved via appropriate scale choices [47] and Sudakov form factors [48] that resum NLL enhancements in the soft and collinear regions of phase space. To this end, in the case of $t\bar{t}$+multijet production, LO partonic events of type $ab \to t\bar{t} + N$ partons are recursively clustered back to a core process $\tilde{a}\tilde{b} \to t\bar{t}$ by means of a k_T jet algorithm [49].

[1] More precisely, the MINLO approach guarantees a consistent resummation of all NLL effects apart from color-suppressed contributions stemming from soft wide angle radiation, which enter $pp \to t\bar{t}$+jets as well as any processes with more than three colored external partons.

The resulting clustering history is interpreted as an event topology, where the N-jet final state emerges from the core process through a sequence of successive branchings that take place at the scales $q_N, \ldots, q_2, q_1$ and are connected by propagators. The nodal scales q_i correspond to the k_T measure of the jet algorithm, and only $1 \to 2$ branchings consistent with the QCD interaction vertices are allowed. In our implementation of the k_T jet algorithm, following [49] we use $\Delta R^2 = 2[\cosh(\Delta y) - \cos(\Delta\phi)]$, where Δy and $\Delta\phi$ denote the rapidity and azimuthal separations, respectively, and we set $R = 0.57$. Typically, the k_T algorithm gives rise to ordered branching histories with $q_1 < \cdots < q_N < \mu_\mathrm{core}$, where μ_core is the characteristic hard scale of the core process. However, also unordered branchings can occur. For instance, this can happen in the presence of jets with transverse momenta above μ_core. Since soft-collinear resummation does not make sense for such hard emissions, in our MINLO implementation possible unordered clusterings are undone and alternative ordered configurations are considered. At the end, the branching history is restricted to ordered branchings $q_1 < \cdots < q_{\tilde{N}} < \mu_\mathrm{core}$, where $\tilde{N} = N - M$. The remaining M jets that cannot be clustered in an ordered way are treated as part of the core process, and μ_core is evaluated according to the kinematics of the corresponding $t\bar{t} + M$ jet hard event.

At LO, the renormalization scale μ_R is chosen according to the event branching history in such a way that

$$[\alpha_\mathrm{s}(\mu_\mathrm{R})]^{N+2} = [\alpha_\mathrm{s}(\mu_\mathrm{core})]^{2+M} \prod_{i=1}^{\tilde{N}} \alpha_\mathrm{s}(q_i), \tag{1}$$

and in our calculation we set $\mu_\mathrm{core} = H_\mathrm{T}/2$.

The resummation of soft and collinear logarithms is achieved by dressing external and internal lines of the event topology by Sudakov form factors. At variance with the original formulation of MINLO [27], in our implementation we employ the symmetry of the LO DGLAP splitting functions, $P_{ab}(z)$, to define physical Sudakov form factors:

$$\Delta_a(Q_0, Q) = \exp\left\{ -\int_{Q_0}^{Q} \frac{\mathrm{d}q}{q} \frac{\alpha_\mathrm{s}(q)}{\pi} \sum_{b=q,g} \times \int_0^{1-q/Q} \mathrm{d}z \left(z\, P_{ab}(z) + \delta_{ab} \frac{\alpha_\mathrm{s}(q)}{2\pi} \frac{2C_a}{1-z} K \right) \right\}, \tag{2}$$

where [50]

$$K = \left(\frac{67}{18} - \frac{\pi^2}{6} \right) C_\mathrm{A} - \frac{10}{9} T_\mathrm{R}\, n_\mathrm{f}, \tag{3}$$

and $a = g, q$ corresponds to massless gluons and quarks, respectively. The representation (2) allows the interpretation of $\Delta_a(Q_0, Q)$ in terms of no-branching probabilities between the scales Q_0 and Q.

Given a LO event topology with $\tilde{N}$ ordered branchings, the lowest branching scale, $q_\mathrm{min} = q_1$, is identified as resolution scale, and the $\tilde{N}$ emissions are supplemented by Sudakov form factors that render them exclusive w.r.t. any extra emissions above q_min. This is achieved by dressing each external line of flavor $a = q, g$ connected with the ith branching by a form factor $\Delta_a(q_\mathrm{min}, q_i)$, while internal lines that connect successive branchings $k < l$ are dressed by factors $\Delta_a(q_\mathrm{min}, q_l)/\Delta_a(q_\mathrm{min}, q_k)$, which correspond to no-branching probabilities between q_k and q_l at resolution scale q_min. For internal lines that connect branchings at q_k to the core process analogous no-branching probabilities between q_k and μ_core are applied. Sudakov form factors along the incoming lines provide a NLL resummation that corresponds to the evolution of PDFs from the resolution scale q_min to the hard scale of the core process. Therefore, for consistency, PDFs are evaluated at the factorization scale $\mu_\mathrm{F} = q_\mathrm{min}$.

The generalization to NLO requires only two straightforward modifications of the LO algorithm. First, for what concerns the scale setting and Sudakov form factors, the contributions that live in the N-parton phase space, i.e. Born and one-loop contributions as well as all IR-subtraction terms, are handled exactly as in LO. Instead, real-emission events that lead to histories with $\tilde{N} + 1 \leq N + 1$ ordered branchings at scales $q_0 < q_1 < \cdots < q_{\tilde{N}}$ are handled as Born-like $\tilde{N}$-parton events with resolution scale $q_\mathrm{min} = q_1$, i.e. the softest branching at the scale q_0 is considered as unresolved and is simply excluded from the MINLO procedure. In other words, the softest emission at NLO is not dressed with Sudakov form factors and does not enter the definitions of μ_R and μ_F. Second, appropriate counterterms are introduced in order to subtract the overall $\mathcal{O}(\alpha_\mathrm{s})$ contribution from Sudakov form factors, such as to avoid double counting of NLO effects.

Concerning the treatment of top quarks a few extra comments are in order. Given the low rate at which top quarks radiate jets, such emissions are simply neglected in our implementation of the MINLO procedure by excluding top quarks from the clustering algorithm. To quantify the uncertainty arising from this approach, we implemented an alternative algorithm that allows the combination of top quarks with other final-state partons in the massive Durham scheme [51,52]. The difference between the two procedures is found to be about 10% at leading order and 5% at next-to-leading order for the observables studied here, and it is therefore smaller than the renormalization and factorization scale uncertainties. Finally, also the top quarks that enter the core process are dressed with Sudakov form factors $\Delta_t(q_\mathrm{min}, \mu_\mathrm{core})$, which render them exclusive w.r.t. emis-

sions above $q_{\min}$. To compute the Sudakov form factors Δ_t, we include quark masses in the splitting functions, according to the method described in [51,52], using the corresponding extension of Eq. (2). This means in particular that we use the massive splitting functions from [53], the propagator corrections listed in [51,52], and we replace the two-loop cusp term $K\, 2C_F/(1-z)$ by $K\, C_F(2/(1-z) - m^2/p_i p_j)$ in the case of massive quark splittings $\widetilde{ij} \to i, j$.

Scale uncertainties in the MINLO framework are assessed through standard factor-two variations of μ_R and μ_F. The renormalization scale is kept fixed in the Sudakov form factors but is varied as usual in the rest of the (N)LO cross section, including the counterterms that subtract the $\mathcal{O}(\alpha_s)$ parts of the Sudakov form factors at NLO. Variations $\mu_F \to \xi_F\, \mu_F$ of the factorization scale are more subtle since $\mu_F = q_{\min}$ plays the role of a matching scale that connects the resummation of QCD radiation via PDF evolution (up to the scale μ_F) with its effective continuation in the form of exclusive matrix-element emissions (above $q_{\min}$) supplemented with initial-state Sudakov form factors. One may either keep $q_{\min}$ as a fixed resolution scale, or redefine $q_{\min} \to \xi_F q_{\min}$. Both methods are perfectly consistent at NLO but problematic for what concerns the resummation of higher-order effects. Keeping $q_{\min}$ fixed formally generates only NNLL corrections, but it implies that the PDF evolution resums resolved QCD radiation above $q_{\min}$ if $\xi_F > 1$. This contradicts the definition of $q_{\min}$ as the resolution scale. Conversely, QCD radiation is not resummed up to $q_{\min}$ if $\xi_F < 1$, again contradicting the definition of $q_{\min}$. On the other hand, varying $q_{\min}$ implies a modified resolution scale $\xi_F q_{\min}$, which is consistent with DGLAP evolution up to $\xi_F \mu_F$ in the PDFs but does not match the scale $q_{\min}$ of the softest exclusive emission as given by the event kinematics. Formally this method generates corrections of NLL type. As a consequence, both types of ξ_F variations are going to alter the logarithmic resummation. To be conservative in our error estimate we decide to apply μ_F variations and simultaneously vary $q_{\min}$.[2] These variations turn out to have a marginal impact on the overall (μ_R, μ_F) scale uncertainties at NLO, and we checked that this applies also to the alternative approach with μ_F variations and fixed $q_{\min}$. However, we have found that scale variations can be enhanced in certain phase-space regions when $q_{\min}$ is kept fixed.

4 Predictions for the 13 TeV LHC

In the following we present selected predictions for $pp \to t\bar{t} + 0, 1, 2, 3$ jets at 13 TeV. We construct jets by clustering light partons with the anti-k_t algorithm [54] at $R = 0.4$, and by default we select jets with pseudorapidity $|\eta_{\text{jet}}| < 2.5$ and a jet-p_T threshold of 25 GeV. Unless stated otherwise, depending on the minimum number N of jets that is required by the observable at hand, inclusive (N)LO or MI(N)LO calculations with N jets are used.

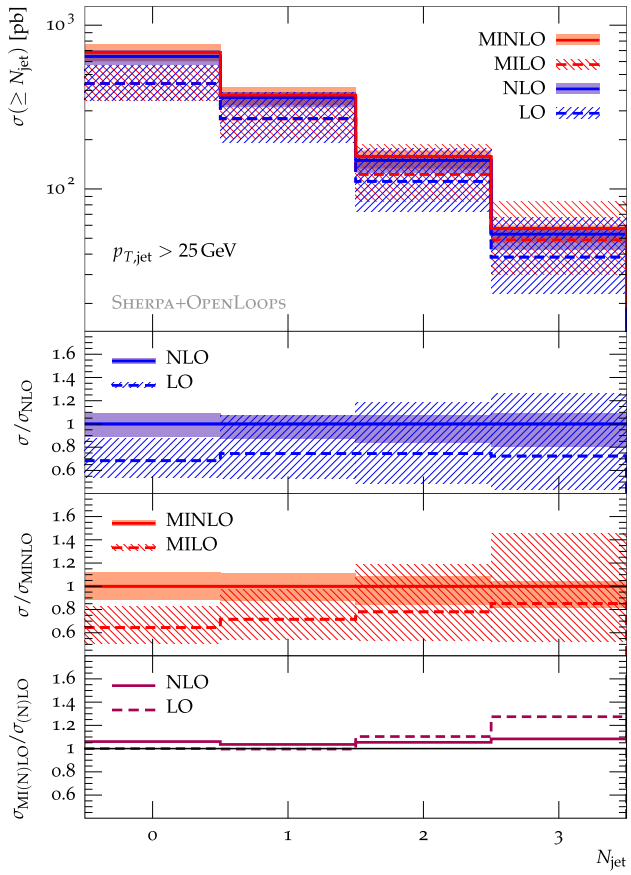

Fig. 1 Inclusive $t\bar{t}$+multijet cross sections with a minimum number $N = 0, 1, 2, 3$ of jets at $p_{T,\text{jet}} \geq 25$ GeV. See the main text for details

The jet multiplicity distribution is presented in Fig. 1. The top panel displays four predictions, stemming from fixed-order LO and NLO calculations, and from MINLO computations at LO and NLO (labeled 'MILO' and 'MINLO'). The second panel shows the ratio between LO and NLO predictions at fixed order, while the third panel shows the ratio between MILO and MINLO predictions. The last panel shows the ratio between MINLO and NLO. The bands illustrate scale uncertainties estimated through independent factor-two rescaling of μ_R and μ_F excluding antipodal variations. Fixed-order predictions feature rather large NLO corrections of about +50% for all jet multiplicities, while MINLO results feature steadily decreasing corrections for increasing N_{jets}. In both cases, LO scale uncertainties tend to grow by more than 10% at each extra jet emission, while (MI)NLO scale uncertainties are significantly reduced and

[2] More precisely, $q_{\min} \to \xi_F\, q_{\min}$ variations are applied only to Sudakov form factors associated with external and internal initial-state lines, and Sudakov form factors $\Delta_a(\xi_F\, q_{\min}, q_k)$ are set to one when $\xi_F\, q_{\min}$ exceeds q_k.

Table 2 Inclusive ($N_{\text{jets}} \geq n$) and exclusive ($N_{\text{jets}} = n$) cross sections with $n = 0, 1, 2, 3$ jets and different transverse momentum thresholds, $p_{\text{T,jet}} \geq 25, 40, 60, 80$ GeV. Uncertainties represent the envelope of the independent μ_{R} and μ_{F} variations around the central value (antipodal variations excluded)

$p_{\text{T,jet}} \geq 25$ GeV	LO	NLO	MILO	MINLO	$\frac{\text{MINLO}}{\text{NLO}}$	$\frac{\text{MINLO}}{\text{MILO}}$	$\frac{\text{NLO}}{\text{LO}}$
$N_{\text{jets}} \geq 0$	$440.46(22)^{+28\%}_{-21\%}$	$644.34(31)^{+9\%}_{-11\%}$	$440.46(22)^{+28\%}_{-21\%}$	$683.21(31)^{+12\%}_{-12\%}$	1.06	1.55	1.46
$N_{\text{jets}} = 0$		$375.36(41)^{+3\%}_{-15\%}$		$394.66(41)^{+2\%}_{-11\%}$	1.05	0.90	0.85
$N_{\text{jets}} \geq 1$	$268.93(9)^{+43\%}_{-28\%}$	$361.01(26)^{+7\%}_{-13\%}$	$267.86(9)^{+36\%}_{-24\%}$	$373.94(23)^{+11\%}_{-13\%}$	1.04	1.40	1.34
$N_{\text{jets}} = 1$		$249.52(27)^{+2\%}_{-17\%}$		$237.88(25)^{+5\%}_{-14\%}$	0.95	0.89	0.93
$N_{\text{jets}} \geq 2$	$111.32(3)^{+59\%}_{-35\%}$	$149.43(16)^{+8\%}_{-16\%}$	$122.86(4)^{+53\%}_{-32\%}$	$157.49(16)^{+9\%}_{-16\%}$	1.05	1.28	1.34
$N_{\text{jets}} = 2$		$111.11(16)^{+1\%}_{-18\%}$		$103.98(17)^{+5\%}_{-21\%}$	0.94	0.85	1.00
$N_{\text{jets}} \geq 3$	$38.36(2)^{+75\%}_{-40\%}$	$53.01(10)^{+9\%}_{-20\%}$	$48.89(2)^{+71\%}_{-38\%}$	$57.43(11)^{+4\%}_{-18\%}$	1.08	1.17	1.38
$N_{\text{jets}} = 3$		$41.12(10)^{+0\%}_{-19\%}$		$38.14(12)^{+5\%}_{-38\%}$	0.93	0.78	1.07
$p_{\text{T,jet}} \geq 40$ GeV	LO	NLO	MILO	MINLO	$\frac{\text{MINLO}}{\text{NLO}}$	$\frac{\text{MINLO}}{\text{MILO}}$	$\frac{\text{NLO}}{\text{LO}}$
$N_{\text{jets}} \geq 0$	$440.46(22)^{+28\%}_{-21\%}$	$644.34(31)^{+9\%}_{-11\%}$	$440.46(22)^{+28\%}_{-21\%}$	$683.21(31)^{+12\%}_{-12\%}$	1.06	1.55	1.46
$N_{\text{jets}} = 0$		$461.03(36)^{+1\%}_{-4\%}$		$483.40(36)^{+1\%}_{-5\%}$	1.05	1.10	1.05
$N_{\text{jets}} \geq 1$	$183.17(7)^{+44\%}_{-28\%}$	$255.88(20)^{+9\%}_{-13\%}$	$200.36(7)^{+35\%}_{-24\%}$	$276.63(20)^{+10\%}_{-12\%}$	1.08	1.38	1.40
$N_{\text{jets}} = 1$		$201.57(20)^{+0\%}_{-8\%}$		$206.41(21)^{+3\%}_{-7\%}$	1.02	1.03	1.10
$N_{\text{jets}} \geq 2$	$54.23(2)^{+59\%}_{-35\%}$	$76.13(8)^{+10\%}_{-17\%}$	$68.34(2)^{+51\%}_{-31\%}$	$84.71(10)^{+6\%}_{-14\%}$	1.11	1.24	1.40
$N_{\text{jets}} = 2$		$62.30(8)^{+0\%}_{-12\%}$		$63.60(10)^{+2\%}_{-14\%}$	1.02	0.93	1.15
$N_{\text{jets}} \geq 3$	$13.84(1)^{+75\%}_{-40\%}$	$19.87(4)^{+11\%}_{-21\%}$	$20.55(1)^{+68\%}_{-37\%}$	$22.70(6)^{+2\%}_{-15\%}$	1.14	1.10	1.44
$N_{\text{jets}} = 3$		$16.61(4)^{+1\%}_{-16\%}$		$16.80(6)^{+0\%}_{-33\%}$	1.01	0.82	1.20
$p_{\text{T,jet}} \geq 60$ GeV	LO	NLO	MILO	MINLO	$\frac{\text{MINLO}}{\text{NLO}}$	$\frac{\text{MINLO}}{\text{MILO}}$	$\frac{\text{NLO}}{\text{LO}}$
$N_{\text{jets}} \geq 0$	$440.46(22)^{+28\%}_{-21\%}$	$644.34(31)^{+9\%}_{-11\%}$	$440.46(22)^{+28\%}_{-21\%}$	$683.21(31)^{+12\%}_{-12\%}$	1.06	1.55	1.46
$N_{\text{jets}} = 0$		$521.32(33)^{+3\%}_{-6\%}$		$547.02(33)^{+5\%}_{-8\%}$	1.05	1.24	1.18
$N_{\text{jets}} \geq 1$	$123.16(5)^{+44\%}_{-29\%}$	$175.69(15)^{+9\%}_{-14\%}$	$142.02(6)^{+35\%}_{-24\%}$	$195.17(17)^{+9\%}_{-12\%}$	1.11	1.37	1.43
$N_{\text{jets}} = 1$		$149.59(16)^{+3\%}_{-10\%}$		$160.41(17)^{+2\%}_{-8\%}$	1.07	1.13	1.21
$N_{\text{jets}} \geq 2$	$26.06(1)^{+59\%}_{-35\%}$	$37.47(5)^{+11\%}_{-18\%}$	$35.24(2)^{+49\%}_{-30\%}$	$43.02(8)^{+4\%}_{-13\%}$	1.15	1.22	1.44
$N_{\text{jets}} = 2$		$32.50(5)^{+4\%}_{-14\%}$		$35.10(8)^{+2\%}_{-9\%}$	1.08	1.00	1.25
$N_{\text{jets}} \geq 3$	$4.95(0)^{+74\%}_{-40\%}$	$7.31(2)^{+13\%}_{-22\%}$	$7.97(1)^{+65\%}_{-36\%}$	$8.61(3)^{+1\%}_{-13\%}$	1.18	1.08	1.48
$N_{\text{jets}} = 3$		$6.41(2)^{+5\%}_{-18\%}$		$6.89(3)^{+1\%}_{-27\%}$	1.07	0.86	1.29
$p_{\text{T,jet}} \geq 80$ GeV	LO	NLO	MILO	MINLO	$\frac{\text{MINLO}}{\text{NLO}}$	$\frac{\text{MINLO}}{\text{MILO}}$	$\frac{\text{NLO}}{\text{LO}}$
$N_{\text{jets}} \geq 0$	$440.46(22)^{+28\%}_{-21\%}$	$644.34(31)^{+9\%}_{-11\%}$	$440.46(22)^{+28\%}_{-21\%}$	$683.21(31)^{+12\%}_{-12\%}$	1.06	1.55	1.46
$N_{\text{jets}} = 0$		$555.85(32)^{+5\%}_{-8\%}$		$584.21(32)^{+7\%}_{-9\%}$	1.05	1.33	1.26
$N_{\text{jets}} \geq 1$	$88.46(4)^{+44\%}_{-29\%}$	$127.22(12)^{+10\%}_{-14\%}$	$104.19(5)^{+34\%}_{-25\%}$	$142.99(14)^{+9\%}_{-12\%}$	1.12	1.37	1.44
$N_{\text{jets}} = 1$		$112.89(12)^{+5\%}_{-12\%}$		$123.77(14)^{+3\%}_{-9\%}$	1.10	1.19	1.28
$N_{\text{jets}} \geq 2$	$14.33(1)^{+59\%}_{-35\%}$	$20.81(3)^{+11\%}_{-18\%}$	$19.90(1)^{+48\%}_{-30\%}$	$24.22(4)^{+3\%}_{-12\%}$	1.16	1.22	1.45
$N_{\text{jets}} = 2$		$18.64(3)^{+6\%}_{-15\%}$		$20.71(4)^{+1\%}_{-9\%}$	1.11	1.04	1.30
$N_{\text{jets}} \geq 3$	$2.17(0)^{+74\%}_{-40\%}$	$3.22(1)^{+13\%}_{-22\%}$	$3.59(0)^{+63\%}_{-36\%}$	$3.85(2)^{+1\%}_{-13\%}$	1.19	1.07	1.48
$N_{\text{jets}} = 3$		$2.91(1)^{+8\%}_{-19\%}$		$3.23(2)^{+1\%}_{-23\%}$	1.11	0.90	1.34

the total width of the (MI)NLO variation bands is about 20–25% for all considered N_{jets} values. Comparing fixed-order NLO and MINLO predictions we observe a remarkable agreement at the level of 4–8%. This supports NLO and MINLO scale-uncertainty estimates based on factor-two variations and encourages the usage of either of the

two calculations (NLO and MINLO) in practical applications.

As demonstrated in Table 2, the good agreement between fixed-order NLO and MINLO results and the consistency of the observed NLO–MINLO differences with factor-two scale variations persist also for a range of other commonly used $p_{\mathrm{T,jet}}$-thresholds [55]. More precisely, for inclusive $t\bar{t}+N$ jet cross sections with jet-p_{T} thresholds of 25, 40, 60 and 80 GeV, MINLO predictions lie systematically above NLO ones. The difference amounts to 6% in the inclusive case and grows up to 19% at large jet multiplicity and for large p_{T}-thresholds, in which case MINLO cross sections feature significantly better perturbative convergence and smaller scale uncertainties as compared to fixed-order ones. This can be attributed to the improved treatment of multijet events with multiple scales through logarithmic resummation in MINLO. In Table 2 also exclusive cross sections with exactly N jets are presented. In that case, the difference between MINLO and NLO predictions varies between -7% and +11%. Apart from the zero-jet case, where the MINLO approach is not well motivated, the MINLO/NLO ratio is almost independent of the number of jets and grows from 0.95 to 1.10 when the p_{T}-threshold increases from 25 to 80 GeV. Similarly as in the inclusive case, at p_{T}-thresholds above 40 GeV MINLO predictions for exclusive N-jet cross sections with $N \geq 2$ feature much better convergence and smaller scale uncertainties w.r.t. fixed order. However, for lower p_{T}-thresholds the opposite is observed, and in the three-jet case the MINLO scale uncertainty becomes twice as large at the NLO one. This can be attributed to the fact that Sudakov logarithms related to the vetoing of NLO radiation are not resummed in the MINLO approach. In spite of this caveat, the general agreement of fixed-order NLO and MINLO results remains remarkably good and typically consistent with respective scale uncertainties. Actually, at large jet multiplicity and p_T, nominal MINLO predictions can lie slightly outside NLO scale variations and/or vice versa, but this tension never exceeds the 5% level, while MINLO and NLO scale variations are found to overlap for all considered observables in Table 2.

Figure 2 shows ratios of inclusive $t\bar{t}+N$ jet cross sections for successive jet multiplicities. Due to the cancelation of various sources of experimental and theoretical uncertainties, such ratios are ideally suited for precision tests of QCD. Corresponding ratios have been widely studied in vector-boson plus multijet production [56,57], where a striking scaling behavior was observed at high jet multiplicity. In the case of $t\bar{t}$+multijet ratios involving up to three jets we find a moderate dependence on the number of jets but no clear scaling. This behavior is rather similar to scaling violations in $V+$multijet production at lower multiplicity and, analogously as for $V+$multijets, can be attributed to the suppression of important partonic channels

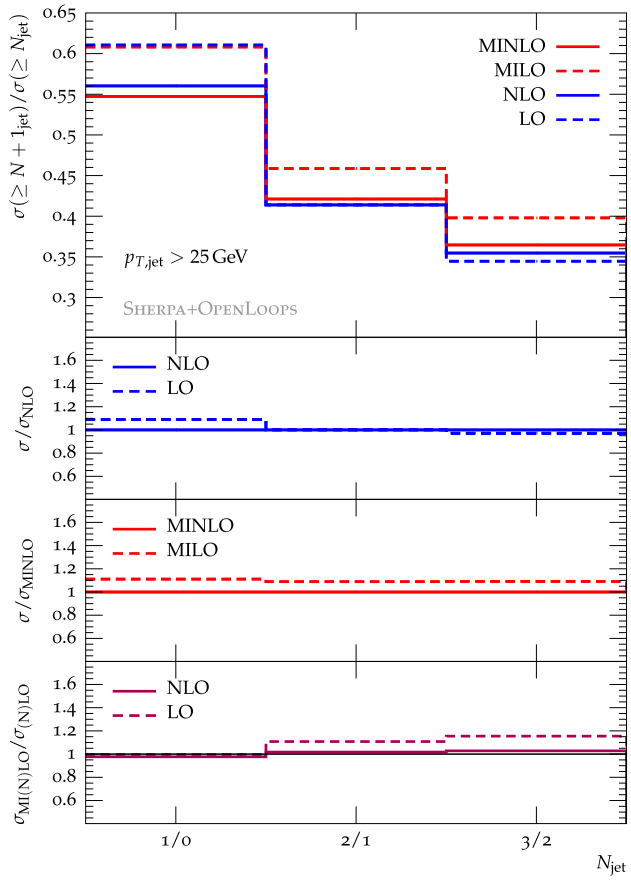

Fig. 2 Ratios of $t\bar{t}+N$ jet over $t\bar{t}+(N-1)$ jet inclusive cross sections for $N=1,2,3$ and $p_{\mathrm{T,jet}} \geq 25$ GeV

in the zero-jet process at LO. In fact, quark–gluon channels are not active in $t\bar{t}$ production at LO. In addition, at LHC energies the gluonic initial state is strongly favored due to the parton luminosity and the t-channel enhancement of the $gg \to t\bar{t}$ cross section, such that the situation becomes similar to vector-boson production, except for the difference of quark versus gluon initial states at LO. When adding additional jets, firstly quark–gluon initial states and secondly quark–quark initial states (including t-channel top-quark diagrams) are added, which contribute sizably to the cross section at larger invariant mass and/or transverse momentum. In order to test scaling hypotheses, it would therefore ultimately be necessary to compute the $t\bar{t}+4$ jet over $t\bar{t}+3$ jet ratio, and eventually the $t\bar{t}+5$ jet over $t\bar{t}+4$ jet ratio. This is out of reach of present technology, therefore we do not investigate the scaling behavior in more detail. Nevertheless, given the excellent agreement between MINLO and NLO predictions up to three jets, the ratios in Fig. 2 can be regarded as optimal benchmarks for precision tests.

Figure 3 shows the transverse momentum spectrum of the top quark for varying jet multiplicities. From low to very high

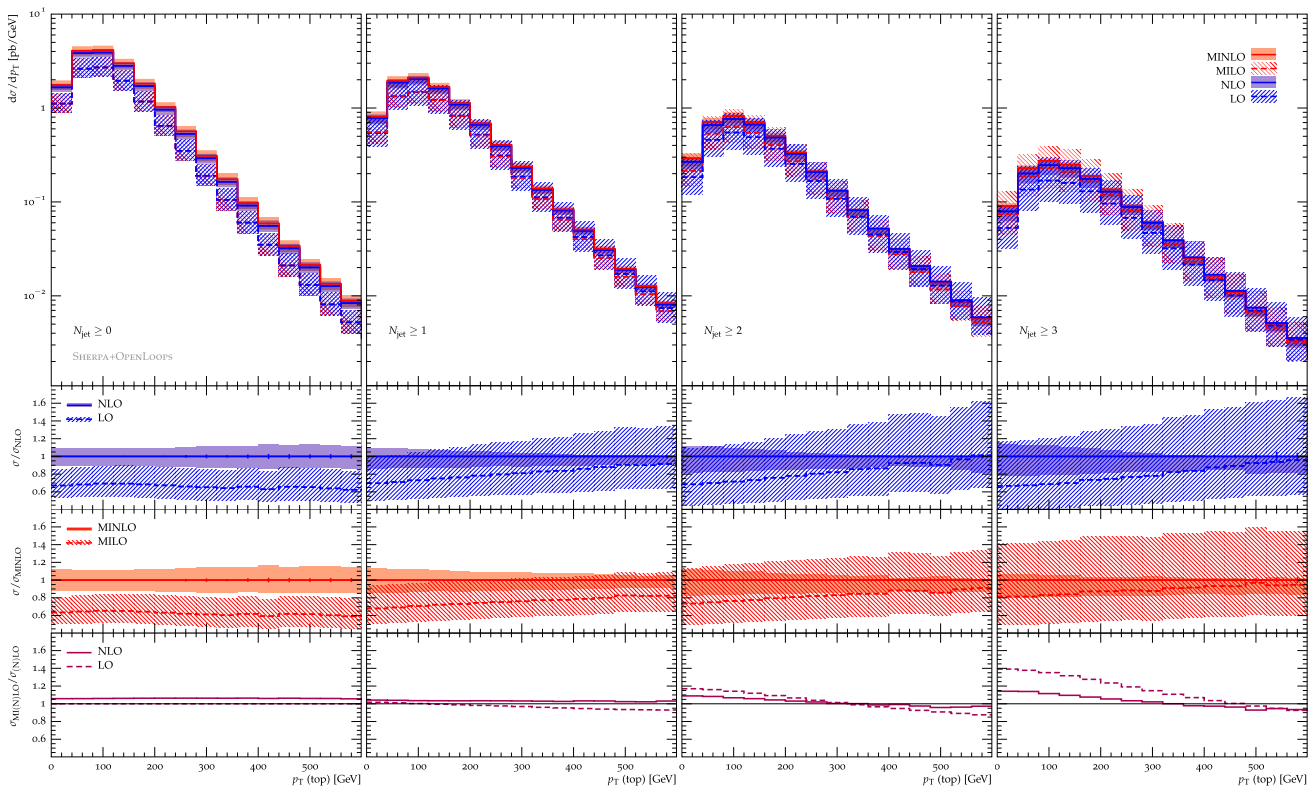

Fig. 3 Distribution in the top-quark p_T for $pp \to t\bar{t} + 0, 1, 2, 3$ jets with $p_{T,\text{jet}} \geq 25\,\text{GeV}$

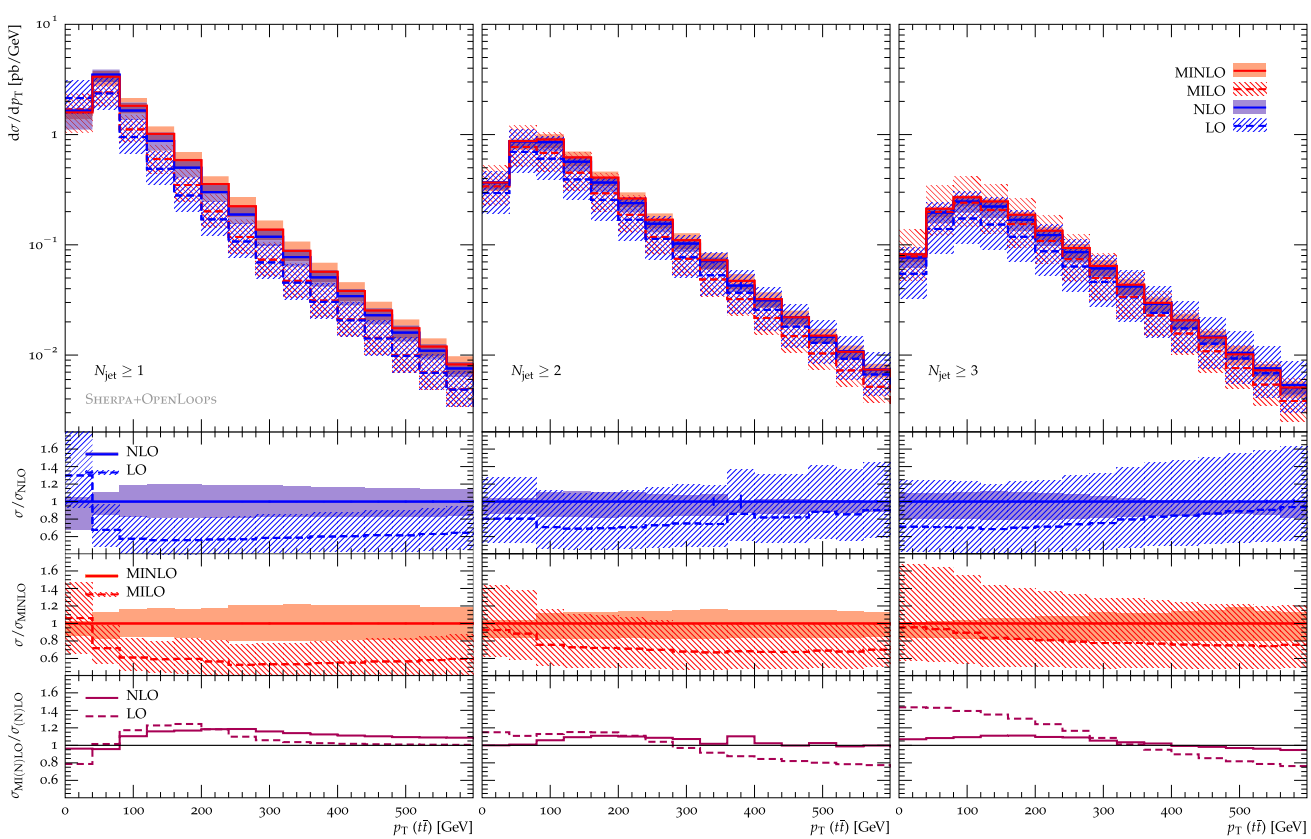

Fig. 4 Distribution in the p_T of the $t\bar{t}$ system for $pp \to t\bar{t} + 1, 2, 3$ jets with $p_{T,\text{jet}} \geq 25\,\text{GeV}$

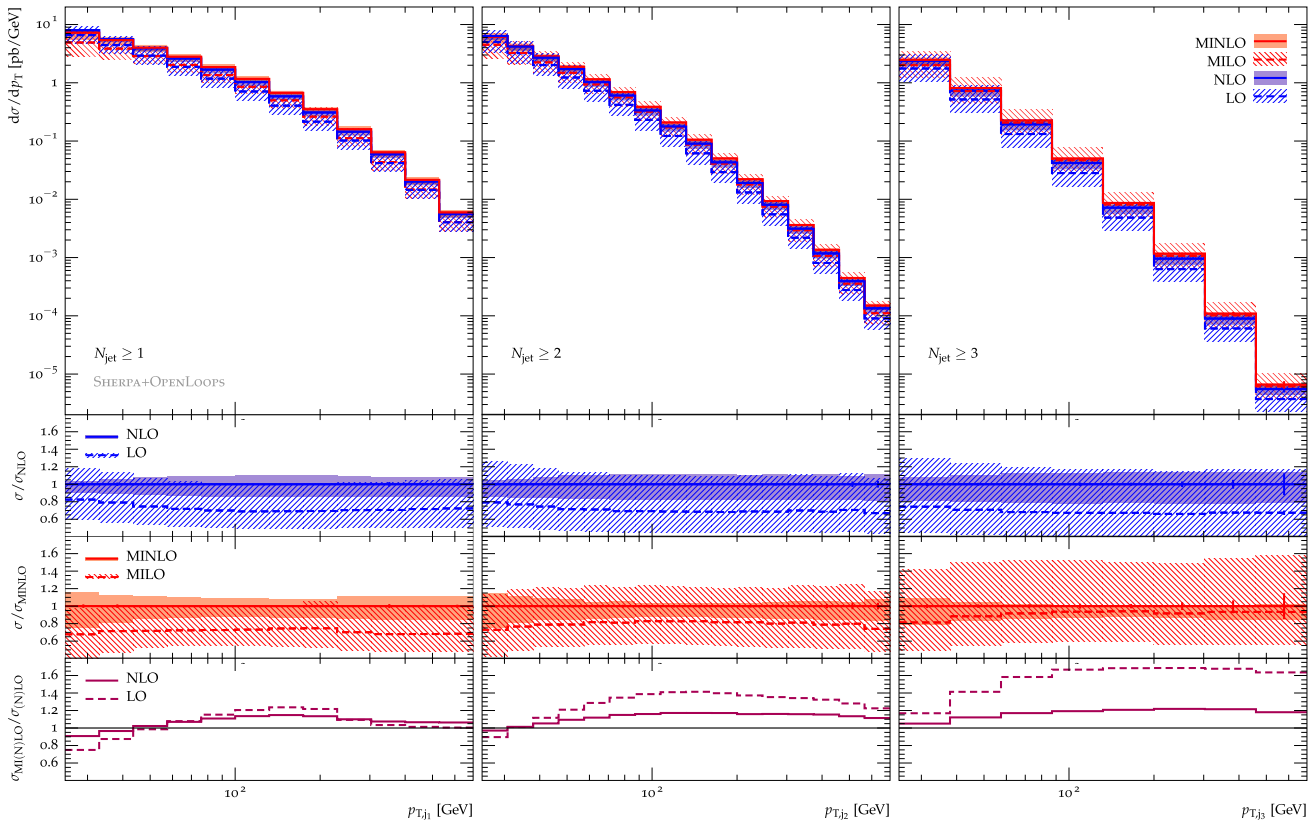

Fig. 5 Distribution in the p_T of the nth jet for $pp \to t\bar{t} + n$ jets with $p_{T,\text{jet}} \geq 25\,\text{GeV}$ and $n = 1, 2, 3$

p_T NLO scale uncertainties remain at a similarly small level as for integrated cross sections. For $N_{\text{jets}} \geq 1$, we observe significant shape corrections, which tend to decrease at high jet multiplicity in MINLO, while in fixed order they remain important. We also observe a shape difference between fixed-order and MINLO predictions, which tends to increase with increasing jet multiplicity but is clearly reduced at NLO. The overall agreement between fixed-order NLO and MINLO results is quite good, both in shape and normalization, with differences that lie within the individual scale uncertainties. Figure 4 shows the top-quark pair transverse momentum spectrum in 1-, 2- and 3-jet samples. We observe a large increase in the cross section between LO and NLO in the one-jet case, where the effect of additional radiation not modeled by the LO calculation is largest. At higher jet multiplicities correction effects tend to decrease. Fixed-order NLO uncertainties are similarly small as in Fig. 3, while MINLO scale uncertainties tend to be more pronounced in the tails. However, we find a very good overall agreement between fixed-order NLO and MINLO predictions, especially for $N_{\text{jets}} \geq 2$ and 3.

The jet transverse momentum spectrum of the first, second and third jet, as predicted by $t\bar{t} + N$ jet calculations of corresponding jet multiplicity, is displayed in Fig. 5. In general we observe approximately constant NLO K-factors over the entire range of transverse momenta analyzed here, but in terms of perturbative convergence and scale uncertainties at NLO we find that the MINLO approach performs better than fixed order. Comparing fixed-order and MINLO results, at LO we find significant deviations that grow with N_{jets} and can reach 60% in the tails. Such differences are largely reduced by the transition to NLO. The fairly decent agreement between fixed-order NLO and MINLO results exemplifies nicely how the convergence of the perturbative series leads to a reduced dependence not only on constant scale variations, but also on the functional form of the scale.

Figure 6 shows inclusive $t\bar{t} + 1, 2, 3$ jet predictions for the total light-jet transverse energy, which is defined as $H_T^{\text{jets}} = \sum_j |p_{T,j}|$, with the sum running over all reconstructed jets within acceptance. This observable is typically badly described by LO calculations, as a sizable fraction of events, especially at large H_T^{jets}, contains additional jets originating in initial-state radiation [58]. Correspondingly we observe a very large increase in the cross section between LO and NLO in the one-jet samples, where the effect of additional radiation not modeled by the calculation is largest. At higher jet multiplicities, the increase is smaller, but well visible. In MINLO it tends to be more pronounced than at fixed order, and for $N_{\text{jets}} \geq 3$ also

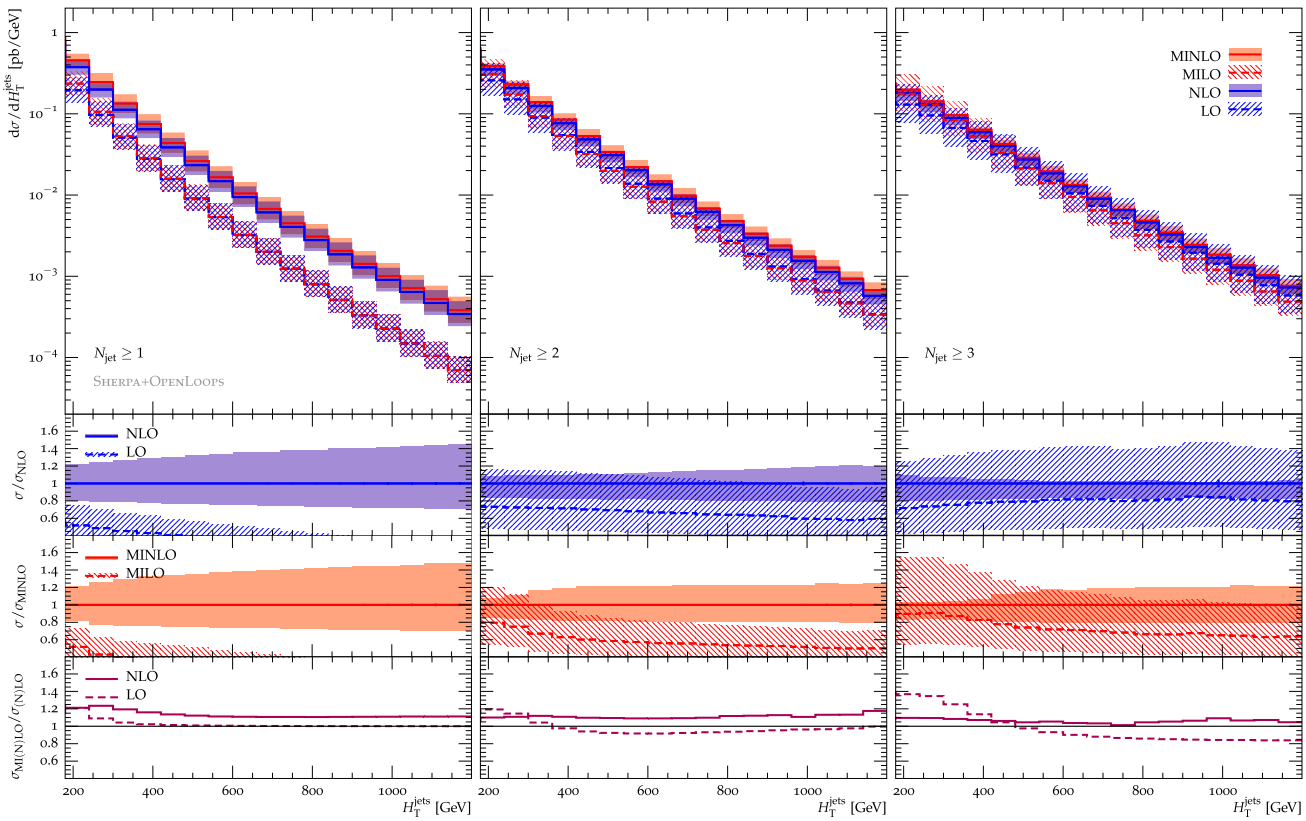

Fig. 6 Distribution in the total transverse energy of light jets for $pp \to t\bar{t} + 1, 2, 3$ jets with $p_{T,jet} \geq 25$ GeV

MINLO uncertainties are larger than NLO ones. Nevertheless, we find good overall agreement between fixed-order NLO and MINLO predictions, independent of the jet multiplicity. However, given the strong sensitivity of H_T^{jets} to multijet emissions, NLO or MINLO calculations with fixed jet multiplicity might significantly underestimate the effect of additional QCD radiation, and an approach like multijet merging at NLO [17] would be more appropriate for this particular observable.

Studying differential distributions in several angular variables we did not find any sizable shape effect. We thus refrain from showing corresponding plots.

5 Conclusions

We have computed predictions for top-quark pair production with up to three additional jets at the next-to-leading order in perturbative QCD using the automated programs OPENLOOPS and SHERPA. This is the first calculation of this complexity involving massive QCD partons in the final state. Given the multi-scale nature of $t\bar{t}$+multijet production, finding a scale that guarantees optimal perturbative convergence is not trivial. Moreover, standard factor-two scale variations might not provide a correct estimate of theoretical uncertainties related to missing higher-order effects. These issues have been addressed by comparing predictions obtained at fixed order using the scale $H_T/2$ and, alternatively, with the MINLO method. The hard scale $H_T/2$ is known to yield good perturbative convergence for a large class of processes, while the MINLO approach is more favorable from the theoretical point of view, as it implements NLL resummation for soft and collinear logarithms that emerge in the presence of large ratios of scales. For a rather wide range of observables at the 13 TeV LHC, we find very good agreement between the predictions generated at fixed order and with the MINLO method. More precisely, MINLO cross sections tend to feature a better perturbative convergence and to lie systematically above NLO ones. But the differences turn out to be well consistent with factor-two scale variations of the respective predictions, which are typically at the 10% level. These findings significantly extend and consolidate the conventional picture of theoretical uncertainties that results from standard scale choices and scale variations.

Acknowledgements We are grateful to A. Denner, S. Dittmaier and L. Hofer for providing us with pre-release versions of the one-loop tensor-integral library COLLIER. This research was supported by the US Department of Energy under contract DE-AC02-76SF00515, by the Swiss National Science Foundation under con-

tracts BSCGI0-157722 and PP00P2-153027, by the Research Executive Agency of the European Union under the Grant Agreements PITN-GA-2012-316704 (*HiggsTools*), by the Kavli Institute for Theoretical Physics through the National Science Foundation's Grant No. NSF PHY11-25915 and by the German Research Foundation (DFG) under Grant No. SI 2009/1-1. We used resources of the National Energy Research Scientific Computing Center, which is supported by the Office of Science of the U.S. Department of Energy under Contract No. DE-AC02-05CH11231.

Open Access This article is distributed under the terms of the Creative Commons Attribution 4.0 International License (http://creativecommons.org/licenses/by/4.0/), which permits unrestricted use, distribution, and reproduction in any medium, provided you give appropriate credit to the original author(s) and the source, provide a link to the Creative Commons license, and indicate if changes were made.
Funded by SCOAP[3].

References

1. M. Czakon, P. Fiedler, A. Mitov, Phys. Rev. Lett. **110**, 252004 (2013). arXiv:1303.6254 [hep-ph]
2. M. Czakon, D. Heymes, A. Mitov, Phys. Rev. Lett. **116**(8), 082003 (2016). arXiv:1511.00549 [hep-ph]
3. S. Dittmaier, P. Uwer, S. Weinzierl, Phys. Rev. Lett. **98**, 262002 (2007). arXiv:hep-ph/0703120
4. A. Bredenstein, A. Denner, S. Dittmaier, S. Pozzorini, Phys. Rev. Lett. **103**, 012002 (2009). arXiv:0905.0110 [hep-ph]]
5. A. Bredenstein, A. Denner, S. Dittmaier, S. Pozzorini, JHEP **03**, 021 (2010). arXiv:1001.4006 [hep-ph]
6. G. Bevilacqua, M. Czakon, C. Papadopoulos, R. Pittau, M. Worek, JHEP **09**, 109 (2009). arXiv:0907.4723 [hep-ph]
7. G. Bevilacqua, M. Czakon, C. Papadopoulos, M. Worek, Phys. Rev. Lett. **104**, 162002 (2010). arXiv:1002.4009 [hep-ph]
8. G. Bevilacqua, M. Czakon, C.G. Papadopoulos, M. Worek, Phys. Rev. D **84**, 114017 (2011). arXiv:1108.2851 [hep-ph]
9. S. Frixione, B.R. Webber, JHEP **06**, 029 (2002). arXiv:hep-ph/0204244
10. S. Frixione, P. Nason, G. Ridolfi, JHEP **09**, 126 (2007). arXiv:0707.3088 [hep-ph]
11. A. Kardos, C. Papadopoulos, Z. Trocsanyi, Phys. Lett. B **705**, 76–81 (2011). arXiv:1101.2672 [hep-ph]
12. S. Alioli, S.-O. Moch, P. Uwer, JHEP **01**, 137 (2012). arXiv:1110.5251 [hep-ph]
13. R. Frederix, S. Frixione, JHEP **12**, 061 (2012). arXiv:1209.6215 [hep-ph]
14. A. Kardos, Z. Trócsányi, J. Phys. **G41**, 075005 (2014). arXiv:1303.6291 [hep-ph]
15. F. Cascioli, P. Maierhöfer, N. Moretti, S. Pozzorini, F. Siegert, Phys. Lett. B **734**, 210–214 (2014). arXiv:1309.5912 [hep-ph]
16. S. Höche, J. Huang, G. Luisoni, M. Schönherr, J. Winter, Phys. Rev. D **88**, 014040 (2013). arXiv:1306.2703 [hep-ph]
17. S. Höche, F. Krauss, P. Maierhöfer, S. Pozzorini, M. Schönherr, F. Siegert, Phys. Lett. B **748**, 74–78 (2015). arXiv:1402.6293 [hep-ph]
18. M. Czakon, H.B. Hartanto, M. Kraus, M. Worek, JHEP **06**, 033 (2015). arXiv:1502.00925 [hep-ph]
19. C.F. Berger, Z. Bern, L.J. Dixon, F. Febres-Cordero, D. Forde, T. Gleisberg, H. Ita, D.A. Kosower, D. Maître, Phys. Rev. Lett. **106**, 092001 (2011). arXiv:1009.2338 [hep-ph]
20. H. Ita, Z. Bern, L.J. Dixon, F. Febres-Cordero, D.A. Kosower, D. Maître, Phys. Rev. D **85**, 031501 (2012). arXiv:1108.2229 [hep-ph]
21. Z. Bern, L. Dixon, F. Febres, Cordero, S. Höche, H. Ita, D.A. Kosower, D. Maître, K.J. Ozeren, Phys. Rev. D **88**, 014025 (2013). arXiv:1304.1253 [hep-ph]
22. S. Badger, B. Biedermann, P. Uwer, V. Yundin, Phys. Rev. D **89**, 034019 (2013). arXiv:1309.6585 [hep-ph]
23. S. Badger, A. Guffanti, V. Yundin, JHEP **1403**, 122 (2014). arXiv:1312.5927 [hep-ph]
24. A. Denner, R. Feger, JHEP **11**, 209 (2015). arXiv:1506.07448 [hep-ph]
25. G. Bevilacqua, H.B. Hartanto, M. Kraus, M. Worek, Phys. Rev. Lett. **116**(5), 052003 (2016). arXiv:1509.09242 [hep-ph]
26. A. Denner, M. Pellen, arXiv:1607.05571 [hep-ph]
27. K. Hamilton, P. Nason, G. Zanderighi, JHEP **1210**, 155 (2012). arXiv:1206.3572 [hep-ph]
28. C.F. Berger, Z. Bern, L.J. Dixon, F. Febres-Cordero, D. Forde, T. Gleisberg, H. Ita, D.A. Kosower, D. Maître, Phys. Rev. D **80**, 074036 (2009). arXiv:0907.1984 [hep-ph]
29. T. Gleisberg, S. Höche, F. Krauss, A. Schälicke, S. Schumann, J. Winter, JHEP **02**, 056 (2004). arXiv:hep-ph/0311263
30. T. Gleisberg, S. Höche, F. Krauss, M. Schönherr, S. Schumann, F. Siegert, J. Winter, JHEP **02**, 007 (2009). arXiv:0811.4622 [hep-ph]
31. F. Cascioli, P. Maierhöfer, S. Pozzorini, Phys. Rev. Lett. **108**, 111601 (2012). arXiv:1111.5206 [hep-ph]
32. F. Cascioli, J. Lindert, P. Maierhöfer, S. Pozzorini, The OpenLoops one-loop generator. http://openloops.hepforge.org
33. G. Ossola, C.G. Papadopoulos, R. Pittau, JHEP **0803**, 042 (2008). arXiv:0711.3596 [hep-ph]
34. A. van Hameren, Comput. Phys. Commun. **182**, 2427–2438 (2011). arXiv:1007.4716 [hep-ph]
35. A. Denner, S. Dittmaier, L. Hofer, arXiv:1604.06792 [hep-ph]
36. A. Denner, S. Dittmaier, Nucl. Phys. B **658**, 175–202 (2003). arXiv:hep-ph/0212259
37. A. Denner, S. Dittmaier, Nucl. Phys. B **734**, 62–115 (2006). arXiv:hep-ph/0509141
38. A. Denner, S. Dittmaier, Nucl. Phys. B **844**, 199–242 (2011)
39. T. Gleisberg, S. Höche, JHEP **12**, 039 (2008). arXiv:0808.3674 [hep-ph]
40. C. Duhr, S. Höche, F. Maltoni, JHEP **08**, 062 (2006). arXiv:hep-ph/0607057
41. S. Catani, M.H. Seymour, Nucl. Phys. B **485**, 291–419 (1997). arXiv:hep-ph/9605323
42. S. Catani, S. Dittmaier, M.H. Seymour, Z. Trocsanyi, Nucl. Phys. B **627**, 189–265 (2002). arXiv:hep-ph/0201036
43. T. Gleisberg, F. Krauss, Eur. Phys. J. C **53**, 501–523 (2008). arXiv:0709.2881 [hep-ph]
44. A. Buckley, J. Butterworth, L. Lönnblad, D. Grellscheid, H. Hoeth et al., Comput. Phys. Commun. **184**, 2803–2819 (2013). arXiv:1003.0694 [hep-ph]
45. S. Dulat, T.J. Hou, J. Gao, M. Guzzi, J. Huston, P. Nadolsky, J. Pumplin, C. Schmidt, D. Stump, C.P. Yuan, Phys. Rev. D **93**(3), 033006 (2016). arXiv:1506.07443 [hep-ph]
46. Z. Bern et al., Comput. Phys. Commun. **185**, 1443–1460 (2014). arXiv:1310.7439 [hep-ph]
47. D. Amati, A. Bassetto, M. Ciafaloni, G. Marchesini, G. Veneziano, Nucl. Phys. B **173**, 429 (1980)
48. S. Catani, Y.L. Dokshitzer, M. Olsson, G. Turnock, B.R. Webber, Phys. Lett. B **269**, 432–438 (1991)
49. S. Catani, Y.L. Dokshitzer, M.H. Seymour, B.R. Webber, Nucl. Phys. B **406**, 187–224 (1993)
50. S. Catani, B.R. Webber, G. Marchesini, Nucl. Phys. B **349**, 635–654 (1991)
51. F. Krauss, G. Rodrigo, Phys. Lett. B **576**, 135–142 (2003). arXiv:hep-ph/0303038
52. G. Rodrigo, F. Krauss, Eur. Phys. J. C **33**, 457–459 (2004). arXiv:hep-ph/0309325

53. S. Catani, S. Dittmaier, Z. Trocsanyi, Phys. Lett. B **500**, 149–160 (2001). arXiv:hep-ph/0011222
54. M. Cacciari, G.P. Salam, G. Soyez, JHEP **04**, 063 (2008). arXiv:0802.1189 [hep-ph]
55. ATLAS collaboration, ATLAS-CONF-2015-065
56. Z. Bern, L. Dixon, F. Febres Cordero, S. Höche, H. Ita, D. Kosower, D. Maître, Phys. Rev. D **92**(1), 014008 (2015). arXiv:1412.4775 [hep-ph]
57. Z. Bern, L.J. Dixon, F. Febres Cordero, S. Höche, H. Ita, D.A. Kosower, D. Maître, K.J. Ozeren, BlackHat Collaboration, PoSLL **011**, 283–288 (2014). arXiv:1407.6564 [hep-ph]
58. M. Rubin, G.P. Salam, S. Sapeta, JHEP **09**, 084 (2010). arXiv:1006.2144 [hep-ph]